CHAPTER EIGHT

The electronic stopping power of heavy targets

Alejandra M.P. Mendez, Darío M. Mitnik, and Claudia C. Montanari*
Institute of Astronomy and Space Physics, CONICET and University of Buenos Aires, Buenos Aires, Argentina
*Corresponding author: e-mail address: mclaudia@iafe.uba.ar

Contents

Abstract

The aim of this work is to face the challenge of describing the stopping power in heavy transition and posttransition metal solids in an extended energy range. The present study examines the stopping of hydrogen in Hf, W, Pb, and Bi. The electronic structure description of the targets requires solving the many-electron Dirac Hamiltonian. We inquire the influence of employing various relativistic approximations, and its effect on the energy loss. The theoretical model of the stopping power considers separately the valence electrons of the metal-accounted for as a free-electron gas and the bound electrons. The former are described using a nonperturbative binary screening potential or the dielectric formalism, depending on the energy regions and plasmon excitation threshold. For the later, the approach uses the dielectric formalism for each subshell by means of the shellwise local plasma approximation. We inspect the importance of accurately describing the 4*f* and 5*d* electrons, the spin–orbit split, the intra- and intershell screening among electrons, and the different quantum dielectric response functions. The present results correctly describe the stopping cross sections in comparison with the data available, the theoretical models DPASS and CasP, and the semiempirical SRIM. Based on these results, we analyze the state of art of the experimental values and suggest the need for new measurements in certain energy ranges and targets.

Advances in Quantum Chemistry, Volume 85
ISSN 0065-3276
https://doi.org/10.1016/bs.aiq.2022.04.005

1. Introduction

The electronic stopping power is a fundamental input of any simulation or experimental research that describes the passage of high energy charged particles through matter. These applications include, among others, ion beam analysis, deposition range and radiation damage; all of them with different technological or medical applications. Providing reliable stopping values for such purposes challenges modern science and encourages the development of accelerator technologies, theoretical modeling, and high performance computing.

Theoretical electronic stopping power calculations go back to the early times of atomic physics.[1–3] Pioneering works by Sabin and coworkers[4] provided useful tabulations for atoms, with shell-by-shell calculations. For molecular targets, the authors considered chemical bonds[5] to improve the usual Bragg rule (addition of the atomic constituents). Many theoretical approaches have been proposed since then. For instance, we can point out the electron–nuclear dynamics to solve the time-dependent Schrödinger equation[6] and the time-dependent density functional theory.[7] Within the binary collision formalism, stand out theories such as the unitary convolution approximation,[8] the binary stopping theory[9] and the self-consistent nonperturbative approach,[10] among others.

A different approach to the inelastic response of the target electrons to the ion passage comes from the quantum dielectric formalism.[11–14] This many-body approximation considers an homogeneous density of non-interacting electrons within the Fermi energy band, including dynamic screening and collective excitations within the limits of the linear response approximation. The dielectric formalism was extended to describe all the target electrons by means of the local plasma approximation (LPA).[15,16] Even though Lindhard's LPA, and its subsequent developments, assume a local response of the bound electrons, it considers the electronic cloud as a whole by using the total electronic density of the atom. Recent proposals[17–19] prove that the models based on the dielectric formalism are still quite efficient to describe the stopping power.

However, despite all the recent theoretical efforts, discrepancies between models and experimental measurements remain present.[20] These differences are originated primarily because the energy loss through matter is a many-body and many-collision phenomena. One of the open problems in the field is the stopping power modeling of systems with nuclear charge $Z_T \geq 55$:

lanthanides, heavy transition metals, and beyond. Recent measurements[21–23] show the limitations of the energy loss models for these heavy targets. A first step toward solving this problem presumes considering a relativistic formalism to describe the electronic structure. In fact, recent theoretical works support this assertion.[24]

In this contribution, we present and discuss the results of the shellwise local plasma approximation (SLPA)[18,25] combined with various relativistic electronic structure calculations. This approximation improves the full dielectric formalism by Chu and Powerd[16] considering independent subshells, as proposed by Meltzer and Sabin,[17] and the ionization threshold of each subshell by using the Levine dielectric function.[26] In fact, the present SLPA surpasses previous versions by introducing the Levine-Mermin dielectric function.[27] The SLPA is a collective model: it takes into account screening among electrons of the same subshell, and also inter-shell screening, when required.[24] This feature constitutes a valuable asset when dealing with the 4*f* and 5*p* subshells of the heavy transition metals. For these targets, the 4*f* and 5*p* electrons are so close in energy that, for impact ions above certain threshold, they respond as a single density of electrons and mutual screening must be considered.

The aim of the present contribution is to study the stopping power in relativistic targets. We examine four illustrative cases: two transition metals, Hf and W, and two posttransition metals, Pb and Bi. These targets include the closed 4*f*-subshell, and open (Hf and W) or closed (Pb and Bi) 5*d*-subshell, while the valence electrons are considered as a free-electron gas (FEG). Detailed electronic structure calculations were performed by implementing nonrelativistic, semirelativistic and fully relativistic approaches. The importance of these calculations to the final stopping values is discussed. Atomic units are employed throughout all this work, unless explicitly stated otherwise.

2. Theoretical description

2.1 The shell-wise local plasma approximation

The many-body consistent treatment for an ion traveling through an homogeneous FEG was developed by Lindhard[11] and by Ritchie[12,14] within the linear response approximation. For the valence electrons of metals we can consider a FEG of density $\rho_{\mathrm{FEG}} = N_e \rho_{at}$, with N_e and ρ_{at} being the number of valence electrons and the atomic density of the solid target, respectively.

The stopping power of a bare ion of charge Z_P moving at velocity v within the FEG is expressed as

$$S_{\mathrm{FEG}} = \frac{2\ Z_P^2}{\pi v^2} \int_0^{\infty} \frac{dk}{k} \int_0^{kv} \omega\ \mathrm{Im}\left[\frac{-1}{\varepsilon(k,\ \omega\ \rho_{\mathrm{FEG}})}\right] d\omega, \tag{1}$$

where $\varepsilon(k, \omega, \rho_{\mathrm{FEG}})$ is the dielectric function. In this work, we employed the Mermin–Lindhard dielectric function,[28] which improves Lindhard's[11] by considering a finite time between electron–electron collisions τ or, equivalently, a damping $\gamma = 1/\tau$. It is worth to underline that this many-electron formalism includes plasmon excitation, with the plasmon frequency being $\omega_p = \sqrt{4\pi\ \rho_{\mathrm{FEG}}}$, as introduced by Lindhard and Scharff.[15] Instead, the value of γ is experimental and related to the energy loss function of the target in the optical limit.[29,30]

Within this formalism, the SLPA[18] describes the response of each *nl* subshell of bound electrons as a gas of electrons of *local* density $\rho_{nl}(r)$ and ionization threshold E_{nl}. The SLPA expression for the energy loss by a bare ion within the atomic cloud of electrons of the *nl* subshell is given by

$$S_{nl} = \frac{2\ Z_P^2}{\pi v^2} \int_0^{\infty} \frac{dk}{k} \int_0^{kv} \omega\ \mathrm{Im}\left[\frac{-1}{\varepsilon_{nl}(k,\ \omega)}\right] d\omega, \tag{2}$$

with

$$\mathrm{Im}\left[\frac{-1}{\varepsilon_{nl}(k,\ \omega)}\right] = \int \mathrm{Im}\left[\frac{-1}{\varepsilon(k,\ \omega,\ \rho_{nl}(r),\ E_{nl})}\right] \mathbf{dr}. \tag{3}$$

The dielectric function $\varepsilon(k,\ \omega,\ \rho_{nl}(r),\ E_{nl})$ is the Levine–Mermin one,[26] which includes explicitly the energy gap E_{nl} to the Mermin dielectric function.[28] The selection of the dielectric function is key since it represents all possible inelastic processes of the bound electrons. Within the SLPA, a local density $\rho_{nl}(r)$ implies a local plasmon frequency $\omega_p^{nl}(r) = \sqrt{4\pi\ \rho_{nl}(r)}$. Following this methodology, a local damping is proposed,[27] given by $\gamma_{nl}(r) = \omega_p^{nl}(r)/2 \equiv \sqrt{\pi\rho_{nl}(r)}$. It is worth mentioning that all the parameters included in the SLPA depend on $\rho_{nl}(r)$ and E_{nl}, which are computed beforehand. This feature maintains the full-theoretical characteristic of the model. As a collective approach, no postmodel shell correction is necessary. The evaluation of Eqs. (2) and (3) is straightforward, with only two inputs values for each *nl* subshell: the electron density (derived from the wave functions) and the binding energy.

2.2 Electronic structure

Since electron densities and binding energies are the only input parameters of the SLPA model, obtaining an accurate description of the target is key. For species with heavy nuclei, whether neutral or ionized, relativistic effects must be included in the computation of the electronic structure. Many methods and numerical codes have been developed to this end; for example, see the reviews by Grant[31] and Fischer et al.[32] In this work, we describe the electronic structure of heavy targets by implementing a nonrelativistic method with relativistic corrections (semirelativistic) and a fully relativistic approach.

The first technique considers the Breit–Pauli (BP) effective Hamiltonian. For a target of N electrons and nuclear charge Z, the BP Hamiltonian is given by,

$$H_{\mathrm{BP}} = H_{\mathrm{NR}} + H_{\mathrm{RC}}, \tag{4}$$

where the first term is the usual nonrelativistic (NR) Hamiltonian

$$H_{\mathrm{NR}} = \sum_{i=1}^{N} h_i + \sum_{i<j} \frac{1}{r_{ij}}, \tag{5}$$

and

$$h_i = -\frac{1}{2}\nabla_i^2 - \frac{Z}{r_i}. \tag{6}$$

The second term correspond to relativistic corrections, composed by one- and two-body terms; see Refs. 33, 34 for more details.

In the second method, the Dirac-Coulomb equation is solved. This Hamiltonian is given by

$$H = \sum_i \left[h_i^{\mathrm{D}} - \frac{Z}{r_i} \right] + \sum_{i<j} \frac{1}{r_{ij}}, \tag{7}$$

where h_i^{D} is the single-electron kinetic Dirac Hamiltonian

$$h_i^{\mathrm{D}} = c\,\boldsymbol{\alpha}_i \cdot \mathbf{p}_i + (\beta_i - 1)c^2, \tag{8}$$

while the remaining terms correspond to the nuclei–electron and electron–electron interaction. Many approaches have been developed to solve Eq. (7); for example, see Refs. 35–37.

3. Results and discussion

For solving the Dirac–Coulomb Hamiltonian, we considered the relativistic version of the parametric potential method developed by Klapisch,[38] which is implemented in the RELAC code and included in the HULLAC suite of codes.[39] We call these calculations R. The full Breit interaction in the Pauli approximation, developed by Eissner et al.,[33] was implemented here by considering the AUTOSTRUCTURE code by Badnell.[40] Within this approach, we used the Thomas–Fermi–Dirac–Amaldi (TFDA) potential,[33,41,42] which features scaling λ_{nl} parameters, and allows adjusting the solutions of Eq. (5). These calculations are denoted as sR. We also implemented a nonrelativistic approach. For this, we used the Hartree–Fock code by Froese Fischer.[43]

The relativistic binding energies (R), the semirelativistic (sR), and the nonrelativistic values (NR) are shown in Fig. 1 for Hf, W, Pb, and Bi. We compare our theoretical calculations with experimental binding energies (measured in solids), compiled by Williams.[44]

Since Fig. 1 displays the binding energies in a five order magnitude range, we add Fig. 2 to discern the discrepancies between the present values and the

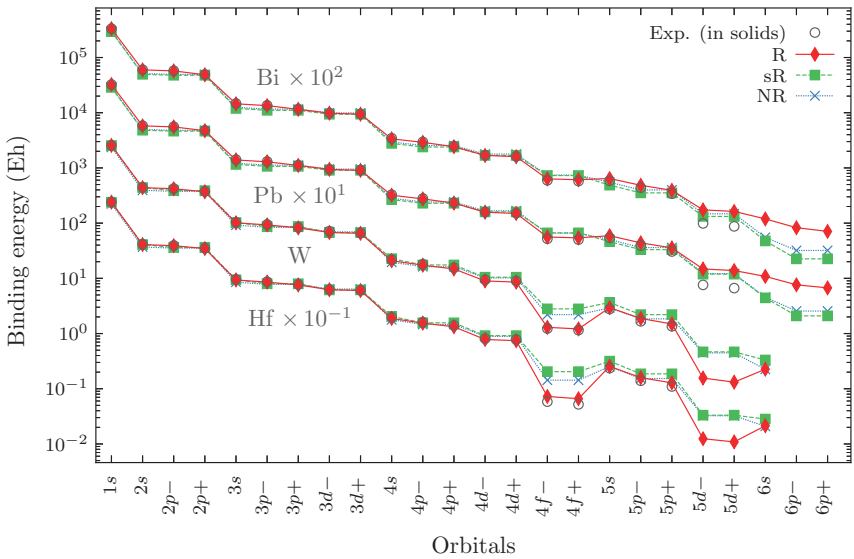

Fig. 1 Binding energy for Hf, W, Pb, and Bi. Symbols: ∘ Experimental data in solids,[44] ◆ relativistic (R), ■ semirelativistic (sR), and × nonrelativistic (NR) values.

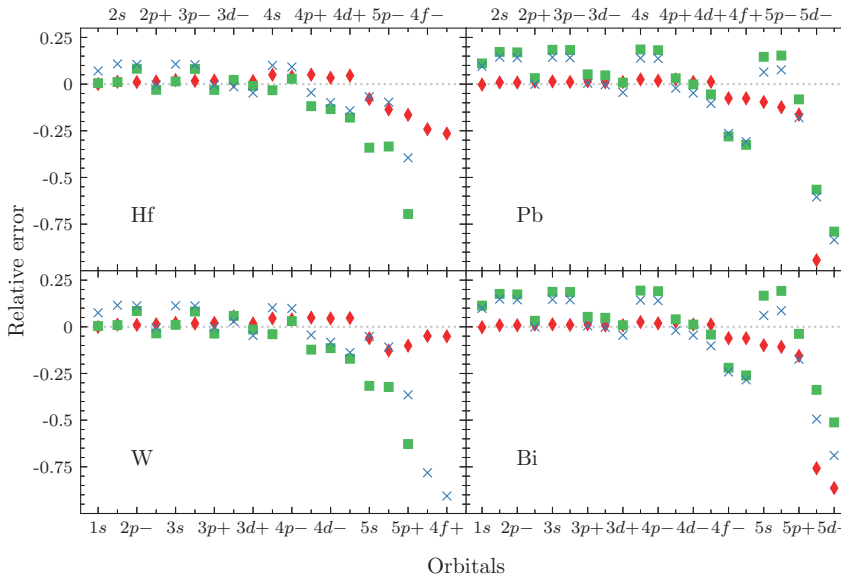

Fig. 2 Binding energy relative error with respect to experimental values for Hf, W, Pb, and Bi. Symbols: same as Fig. 1.

measurements. Binding energy relative errors are given in Fig. 2 for Hf, W, Pb, and Bi. The missing orbital data in the figure correspond to values smaller than −1. For the inner shells, i.e., 1*s*-5*s* for Hf and W and 1*s*-5*d* for Pb and Bi, the semirelativistic calculations and nonrelativistic ones are fairly similar, with a ∼9% agreement, while the relativistic binding energy calculations coincide with the experimental values in about 3%. As expected, the inclusion of relativistic effects are responsible for these improvements. The overall good agreement of the relativistic calculations demonstrates the necessity of including properly the relativistic effects in the structure calculations. As it will be shown later, some of the outer electron wavefunctions have a non-negligible overlap with the internal ones. Therefore, the relativistics effects spread all over the full structure calculation, including the outer-shells. There are some discrepancies for the 5*p* and 4*f* electrons, in the case of Hf and W, and for the 5*p* and 5*d* subshells in Pb and Bi, which can be understood if one recalls that the theoretical calculations assume isolated atoms, whereas the experimental data were taken from the targets in solid state.

In Fig. 3, we display the most outer shells of Hf, W, Pb, and Bi. As can be noticed, the 5*d* and 6*s*, in Hf and W, and the 6*s* and 6*p* electrons, in Pb and Bi, are part of the FEG. For these subshells, the binding energies displayed in

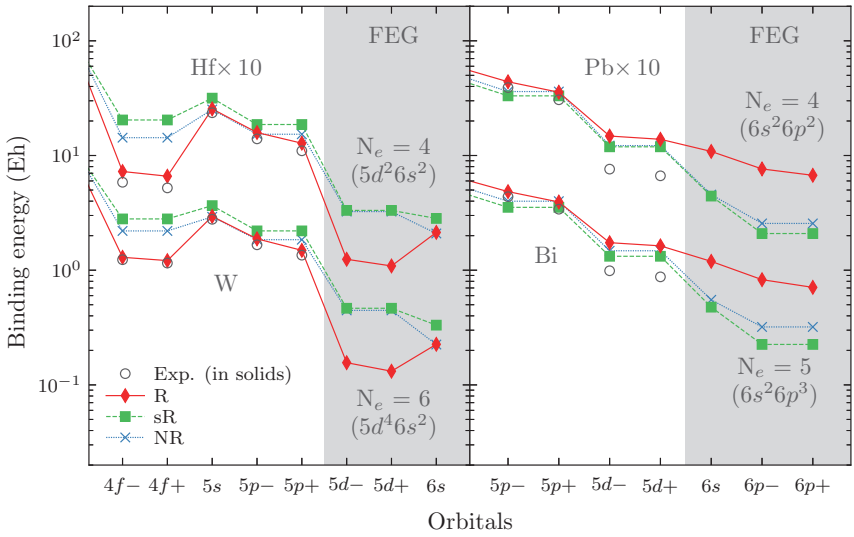

Fig. 3 Binding energy and number of electrons in FEG considered for Hf, W, Pb, and Bi. Symbols: same as Fig. 1.

Fig. 3 only have sense for atoms but not for solids. No experimental values in solids are available, as expected, because these electrons belong to the conduction band. Moreover, these results for the electronic structure are coherent with the expected number of electrons in the FEG, i.e., $N_e = 4$ for Hf and Pb, $N_e = 5$ for Bi, and $N_e = 6$ for W.

The semirelativistic (sR) calculation shown in Figs. 1 and 3 can be further improved by optimizing the λ_{nl} radial scaling parameters that define the TFDA potential employed. There are many approaches to this end; in particular, we manually adjusted the values of λ_{nl} so that the computed binding energies are the same as the experimental measurements. The optimized calculation, denoted sR*, is not shown in Figs. 1 and 3. To illustrate this result, we present in Fig. 4 the calculated densities and mean radius of the inner subshells of Pb. For the relativistic data, the reduced electron density is given by $d_{nl}(r) = P_{nl}(r)^2 + Q_{nl}(r)^2$, where P and Q are the strong and weak components of the reduced radial wavefunction ($\int_0^\infty d_{nl}(r)\, dr = 1$). To simplify this analysis, we have considered a split-orbit average for the nlj subshells. The right panel in Fig. 4 shows that the NR mean radius of the core electron's radial distributions are generally larger than the R, sR and sR* results, as expected. We can observe that the radial distribution of the sR* calculations are also influenced by the optimization. For most of the inner shells,

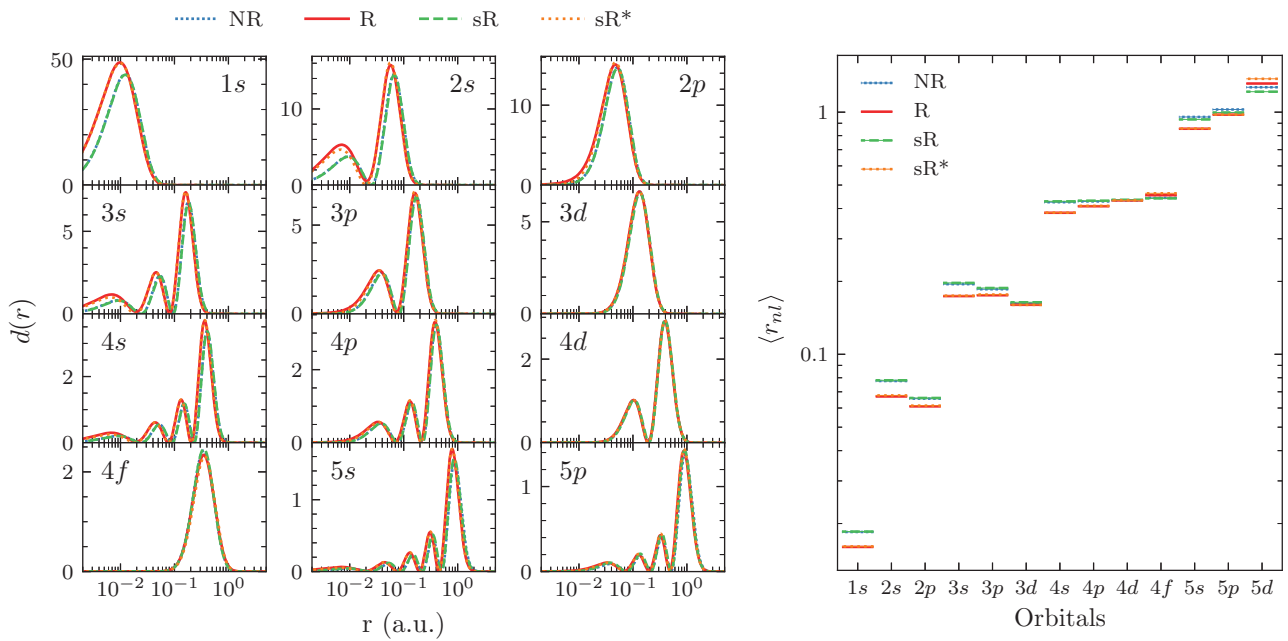

Fig. 4 Present relativistic (R), semirelativistic (sR), optimized semirelativistic (sR*), and nonrelativistic (NR) atomic structure results for Pb. *Left*: Reduced radial electron density for 1*s* to 5*p* subshells (5*d* not included for simplicity). *Right*: mean radius for each subshell.

these results follow the correct behavior: the optimized electron densities are pulled toward the nuclei. The analysis of the differences in the $4f$ and $5d$ subshells surpasses the scope of this work.

In what follows, we present stopping cross sections for Hf, W, Pb, and Bi. The total stopping is obtained by calculating separately the contribution of valence (FEG) and bound electrons, given by Eqs. (1) and (2), respectively. The density ρ_{nl} used in Eq. (3) is related to the reduced electron density d_{nl} by $\rho_{nl}(r) = N_{nl}d_{nl}(r)/r^2$, with N_{nl} being the number of electrons in the subshell nl. Three formalisms are combined to obtain the total stopping cross sections. The first one considers a nonperturbative description of the energy loss in the FEG, based on an screening potential SPCC.[25] This model relies on the binary collisional theory, so no collective excitations (plasmons) are included. The second one calculates the stopping power of the FEG by using Mermin–Lindhard[28] dielectric formalism (ML), which follows a perturbative approximation but includes collective excitations in the energy region, where the plasmon contribution is important. Finally, the third approach combines the SLPA and relativistic electronic structure computations described above.

The first step in the total stopping calculation consists on determining how many electrons are included in the FEG, while the rest are assumed bound to the atom. To make this decision, we considered the relativistic results displayed in Fig. 3. In previous works,[45,46] we based this choice on external experimental values from energy loss measurements in the optical limit. In this contribution, we decided to rely on our full-theoretical developments. Other important improvement constitutes the introduction of the Levine-Mermin dielectric function, which is critical for many target subshells. It is worth mentioning that, in all our calculations, the H projectiles are considered as protons. This characterization is based on two physical processes: (i) Inside the solid, at low impact energies, the dynamic screening of the ion by the FEG prevents any electron to occupy the $1s$ bound state of H.[47] (ii) At high energies, the probability of projectile ionization is more important than capture, so the hydrogen looses the only bound electron in few collisions and arrives to an equilibrium charge state of $Z_P = 1$. For hydrogen projectiles, this charge state is also considered in other calculations like SRIM[48,49] but these are based on the empirical stopping results.

In Fig. 5, we display the present results for H in Hf. The total stopping agrees quite well with the experimental data, suggesting a maximum around 70 keV/amu. Separate curves for the FEG and bound electrons contributions are displayed, together with the total value. As mentioned before,

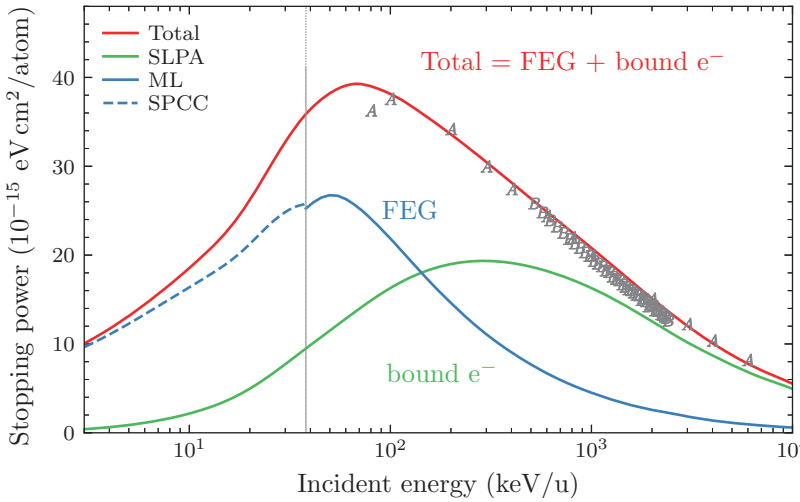

Fig. 5 Stopping power of H on Hf. The contribution of bound electrons and FEG is displayed separately (see acronyms from inset in text). Symbols, experimental data as in IAEA database[50]: A[51] and B.[24]

the FEG curve results from the combination of the SPCC at low energies (dashed line) and the ML at intermediate and high energies. The vertical line illustrates the threshold energy for plasmon excitations.[25,47] The recent version of the SLPA, which considers a local damping,[27] and the present relativistic calculations are employed, improving previous results obtained in Montanari et al.[24]

In Figs. 6–9, we show a set of four total stopping cross sections calculations for H on Hf, W, Pb, and Bi, respectively. In the following, we analyze the importance of the electronic structure calculations by comparing relativistic, semirelativistic and nonrelativistic results. We also include comparison with the semiempirical values by Ziegler's SRIM code,[48,49] the theoretical results by Schiwietz and Grande's code CasP version 6.0 for $Z_P = 1$,[52,53] and the Sigmund and Schinner's DPASS[54,55] curve.

For Hf, no experimental data are available for impact energies around the maximum and below. It can be noted in Fig. 6 that the differences between NR and R are not dramatic, being the former smaller than the latter and with a maximum value slightly shifted to higher energies. On the other hand, the sR and sR* curves are quite different, but neither of them agree with the experimental data. If one recalls Fig. 3, it becomes evident that the more binded are the electrons of the subshell below the FEG (following the experimental description), the larger the cross section.

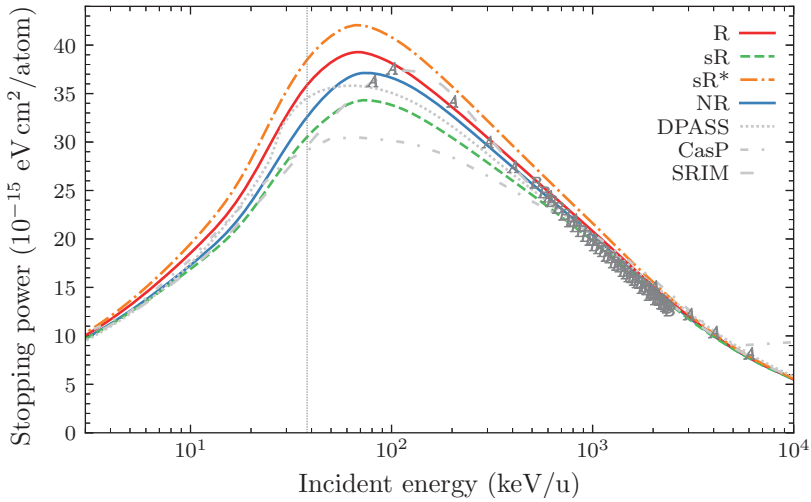

Fig. 6 Stopping power of H on Hf. Present results using relativistic and nonrelativistic electronic structure calculations for bound electrons. In gray theoretical curves CASP[52] and DPASS,[54] and semiempirical values by SRIM.[48] Details in the figure inset. Symbols, experimental data as in IAEA database[50]: A[51] and B.[24]

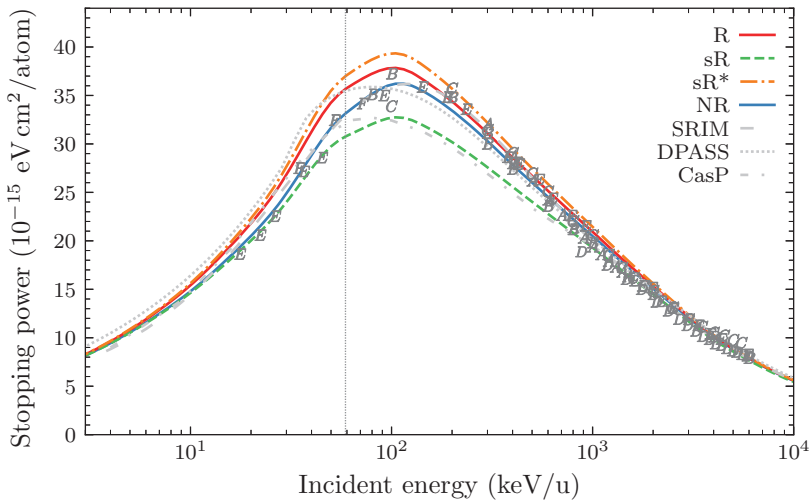

Fig. 7 Stopping power of H on W. Curves as in Fig. 6. Symbols, experimental data as in IAEA database[50]: A,[56] B,[51] C,[57] D,[58] E,[23] and F[23] (for D^+ in W).

Similar results are obtained for H on W, as displayed in Fig. 7. However, recent measurements by Moro et al.[23] (represented with letters E and F in Fig. 7) agree better with the NR results for energies below the maximum.

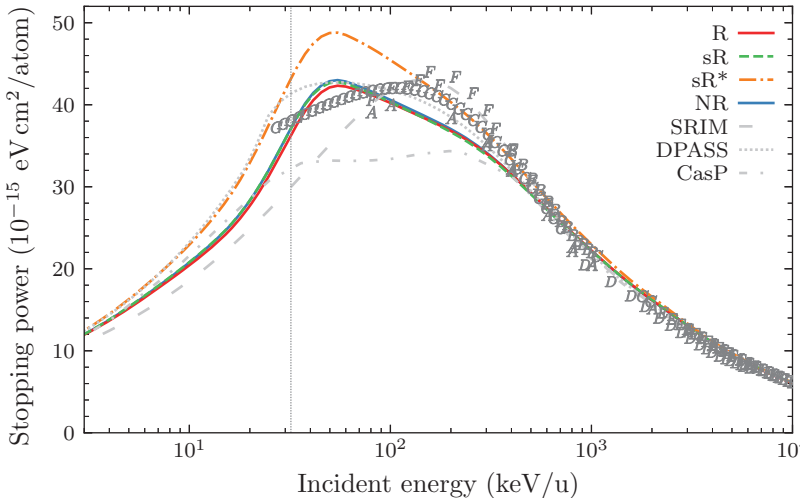

Fig. 8 Stopping power of H on Pb. Curves as in Fig. 6. Symbols, experimental data as in IAEA database[50]: A,[51] B,[59] C,[60] D,[58] E,[61] F,[62] G,[63] H,[64] I,[65] J,[66] and K.[67]

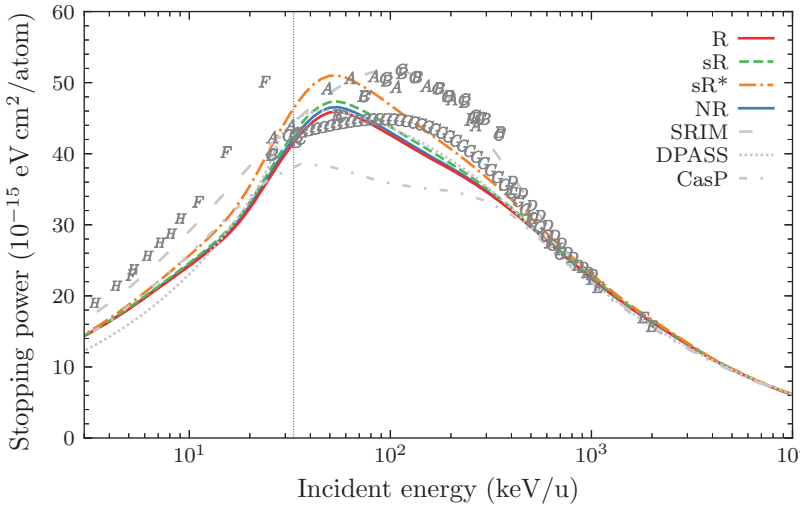

Fig. 9 Stopping power of H on Bi. Curves as in Fig. 6. Symbols, experimental data as in IAEA database[50]: A,[68] B,[69] C,[70] D,[59] E,[60] F,[71] G,[72] H,[73] and I.[74]

The comparison with other theoretical and semiempirical curves shows that DPASS[54] is the closest to our results. It is worth mentioning that for Hf and W, the 4*f* electrons are close in energy to the 5*p* electrons. The SLPA includes the screening among electrons of similar binding energy. For these

cases, inter-shell 5*p*-4*f* screening is included considering the small difference between the binding energies and the meantime for the ion to get through the subshells, as discussed in Ref. 24.

The results for Pb and Bi are different. As can be noted in Fig. 3, the closed 5*d* subshell is located just below the FEG and, consequently, it becomes the main contribution to the stopping power around the maximum. The theoretical structure calculation of such multielectronic targets is a difficult task; particularly for the outer electrons. We can observe in Figs. 8 and 9 that the NR, sR and R calculations are very similar, which follows the corresponding binding energy comparison in Fig. 3. Moreover, these values are close to other models, such as DPASS.[54] The double maximum shape of our R curves indicates that the bound electron contribution could be underestimated. The difference between theoretical (deeper) and experimental (smaller) binding energy for the 5*d* subshell may explain this. In fact, the sR*, which agrees the 5*d* experimental binding energy, describes better the data for impact energies below 500 keV/amu. It should be noted that the latest data on Bi and Pb, for energies around the stopping maximum and below, were measured 30 years ago. Bi and Pb are exceptional cases and new experimental efforts at impact energies below 200 keV are encouraged to clarify these differences.

4. Conclusions

In this contribution, we advanced in the theoretical description of the target's electronic structure by using the best relativistic descriptions available. The combination of these results with the dielectric formalism, the SLPA and the nonperturbative model based on the screened potential allowed us to predict stopping values in an extent energy region. Hf and W were examined to illustrate postlanthanides transition metals, while Pb and Bi exemplified the posttransition metals of the group *p*. The present stopping power results are compared with the experimental data available, and other theoretical and semiempirical models. The influence of the 4*f* electrons (of Hf and W) and the 5*d* electrons (of Pb and Bi) is discussed. From the stopping cross sections analysis, we show that even though there are limitations in the atomic structure approximations, doubts rise over certain experimental values around the stopping maximum. It is obvious from the present analysis that the disagreement among data sets makes it imperative to count on independent theoretical models. Of course, semiempirical models will adapt to the existing data, and this is valid, as far as the existing

measurements are correct. However, for the targets considered here, our model provides one of the best fully theoretical description available.

Acknowledgments

The authors acknowledge the financial support of Consejo Nacional de Investigaciones Científicas y Tecnológicas, Agencia Nacional de Promoción de la Investigación, el Desarrollo Tecnológico y la Innovación, and Universidad de Buenos Aires. The authors thanks Jorge Miraglia for previous discussions on this subject.

References

1. Rosenblum, S. Recherches Expérimentales sur le Passage des Rayons Travers la Matière. *Ann. Phys.* **1928**, *10* (10), 408–471. https://doi.org/10.1051/anphys/192810100408.
2. Bethe, H. Zur Theorie des Durchgangs schneller Korpuskularstrahlen durch Materie. *Ann. Phys.* **1930**, *397* (3), 325–400. https://doi.org/10.1002/andp.19303970303.
3. Bohr, N. *The Penetration of Atomic Particles Through Matter*; Munksgaard Copenhagen, 1948.
4. Oddershede, J.; Sabin, J. R. Orbital and Whole-Atom Proton Stopping Power and Shell Corrections for Atoms With $Z \leq 36$. *At. Data Nucl. Data Tables* **1984**, *31* (2), 275–297. https://doi.org/10.1016/0092-640X(84)90024-X.
5. Oddershede, J.; Sabin, J. R. Bragg Rule Additivity of Bond Stopping Cross Sections. *Nucl. Instrum. Methods Phys. Res. Sect. B* **1989**, *42* (1), 7–10. https://doi.org/10.1016/0168-583X(89)90003-7.
6. Cabrera-Trujillo, R.; Sabin, J. R.; Deumens, E.; Öhrn, Y. Dynamical Processes in Stopping Cross Sections. In *Theory of the Interaction of Swift Ions With Matter. Part 1*; Advances in Quantum Chemistry, Vol. 45; Academic Press, 2004; pp. 99–124. https://doi.org/10.1016/S0065-3276(04)45005-9.
7. Quashie, E. E.; Andrade, X. A. A. C. Directional Dependency of Electronic Stopping in Nickel, Projectile'S Excited Charge State and Momentum Transfer. *Eur. Phys. J. D* **2021**, *75*, 280. https://doi.org/10.1140/epjd/s10053-021-00266-6.
8. Schiwietz, G.; Grande, P. Stopping of Protons – Improved Accuracy of the UCA Model. *Nucl. Instrum. Methods Phys. Res. Sect. B* **2012**, *273*, 1–5. https://doi.org/10.1016/j.nimb.2011.07.023 (20th International Conference on Ion Beam Analysis).
9. Sigmund, P.; Schinner, A. Progress in Understanding Heavy-Ion Stopping. *Nucl. Instrum. Methods Phys. Res. Sect. B* **2016**, *382*, 15–25. https://doi.org/10.1016/j.nimb.2015.12.041 (The 21st International workshop on Inelastic Ion Surface Collisions (IISC-21)).
10. Arista, N. R. Energy Loss of Ions In Solids: Non-Linear Calculations for Slow and Swift Ions. *Nucl. Instrum. Methods Phys. Res. Sect. B* **2002**, *195* (1), 91–105. https://doi.org/10.1016/S0168-583X(02)00687-0.
11. Lindhard, J. On the Properties of a Gas of Charged Particles. *K. Dan. Vidensk. Selsk. Mat.-Fys. Medd.* **1954**, *28* (8).
12. Ritchie, R. H. Interaction of Charged Particles With a Degenerate Fermi-Dirac Electron Gas. *Phys. Rev.* **1959**, *114* (3), 644–654. https://doi.org/10.1103/PhysRev.114.644.
13. Echenique, P. M.; Brandt, W.; Ritchie, R. H. Self-Consistent Wake Binding Energies. *Phys. Rev. B* **1986**, *33* (1), 43–48. https://doi.org/10.1103/PhysRevB.33.43.
14. Echenique, P. M.; Flores, F.; Ritchie, R. H. Dynamic Screening of Ions in Condensed Matter. In *Solid State Physics*; Ehrenreich, H., Turnbull, D., Eds.; Vol. 43; Academic Press, 1990; pp. 229–308. https://doi.org/10.1016/S0081-1947(08)60325-2.

15. Lindhard, J.; Scharff, M. Energy Loss in Matter by Fast Particles of Low Charge. *K. Dan. Vidensk. Selsk. Mat.-Fys. Medd.* **1953**, *27* (15), 1–31.
16. Chu, W. K.; Powerd, D. Calculation of Mean Excitation Energy for All Elements. *Phys. Lett. A* **1972**, *40* (1), 23–24. https://doi.org/10.1016/0375-9601(72)90181-8.
17. Meltzer, D. E.; Sabin, J. R.; Trickey, S. B. Calculation of Mean Excitation Energy and Stopping Cross Section in the Orbital Local Plasma Approximation. *Phys. Rev. A* **1990**, *41* (1), 220–232. https://doi.org/10.1103/PhysRevA.41.220.
18. Montanari, C. C.; Miraglia, J. E. The Dielectric Formalism for Inelastic Processes in High-Energy Ion-Matter Collisions. In *Advances in Quantum Chemistry: Theory of Heavy Ion Collision Physics in Hadron Therapy*; Belkic, D., Ed.; Vol. 2; Elsevier: New York, 2013; pp. 165–201 (Chapter 7).
19. de Vera, P.; Abril, I.; Garcia-Molina, R. Energy Spectra of Protons and Generated Secondary Electrons Around the Bragg Peak in Materials of Interest in Proton Therapy. *Radiat. Res.* **2018**, *190* (3), 282–297. https://doi.org/10.1667/RR14988.1.
20. Montanari, C.; Dimitriou, P. The IAEA Stopping Power Database, Following the Trends in Stopping Power of Ions in Matter. *Nucl. Instrum. Methods Phys. Res. Sect. B* **2017**, *408*, 50–55. https://doi.org/10.1016/j.nimb.2017.03.138 (Proceedings of the 18th International Conference on the Physics of Highly Charged Ions (HCI-2016), Kielce, Poland, 11–16 September 2016).
21. Roth, D.; Bruckner, B.; Moro, M. V.; Gruber, S.; Goebl, D.; Juaristi, J. I.; Alducin, M.; Steinberger, R.; Duchoslav, J.; Primetzhofer, D.; Bauer, P. Electronic Stopping of Slow Protons in Transition and Rare Earth Metals: Breakdown of the Free Electron Gas Concept. *Phys. Rev. Lett.* **2017**, *118* (10), 103401. https://doi.org/10.1103/PhysRevLett.118.103401.
22. Selau, F. F.; Trombini, H.; Marmitt, G. G.; de Andrade, A. M. H.; Morais, J.; Grande, P. L.; Alencar, I.; Vos, M.; Heller, R. Stopping and Straggling of 60-250-keV Backscattered Protons on Nanometric Pt Films. *Phys. Rev. A* **2020**, *102* (3), 032812. https://doi.org/10.1103/PhysRevA.102.032812.
23. Moro, M. V.; Wolf, P. M.; Bruckner, B.; Munnik, F.; Heller, R.; Bauer, P.; Primetzhofer, D. Experimental Electronic Stopping Cross Section of Tungsten for Light Ions in a Large Energy Interval. *Nucl. Instrum. Methods Phys. Res. Sect. B* **2021**, *498*, 1–8. https://doi.org/10.1016/j.nimb.2021.04.010.
24. Montanari, C. C.; Miranda, P. A.; Alves, E.; Mendez, A. M. P.; Mitnik, D. M.; Miraglia, J. E.; Correa, R.; Wachter, J.; Aguilera, M.; Catarino, N.; da Silva, R. C. Stopping Power of Hydrogen in Hafnium and the Importance of Relativistic 4*f* Electrons. *Phys. Rev. A* **2020**, *101* (6), 062701. https://doi.org/10.1103/PhysRevA.101.062701.
25. Montanari, C. C.; Miraglia, J. E. Low- and Intermediate-Energy Stopping Power of Protons and Antiprotons in Solid Targets. *Phys. Rev. A* **2017**, *96* (1), 012707. https://doi.org/10.1103/PhysRevA.96.012707.
26. Levine, Z. H.; Louie, S. G. New Model Dielectric Function and Exchange-Correlation Potential for Semiconductors and Insulators. *Phys. Rev. B* **1982**, *25* (10), 6310–6316. https://doi.org/10.1103/PhysRevB.25.6310.
27. Peralta, J. P.; Fiori, M.; Mendez, A. M. P.; et al. Stopping Power Calculations and the Levine-Mermin Dielectric Function for Inner Shells. *Phys. Rev. A* **2022**, *105*, 062814. https://doi.org/10.1103/PhysRevA.105.062814.
28. Mermin, N. D. Lindhard Dielectric Function in the Relaxation-Time Approximation. *Phys. Rev. B* **1970**, *1* (5), 2362–2363. https://doi.org/10.1103/PhysRevB.1.2362.
29. Werner, W. S. M.; Glantschnig, K.; Ambrosch-Draxl, C. Optical Constants and Inelastic Electron-Scattering Data for 17 Elemental Metals. *J. Phys. Chem. Ref. Data* **2009**, *38* (4), 1013–1092. https://doi.org/10.1063/1.3243762.

30. Abril, I.; Garcia-Molina, R.; Denton, C. D.; Pérez-Pérez, F. J.; Arista, N. R. Dielectric Description of Wakes and Stopping Powers in Solids. *Phys. Rev. A* **1998**, *58* (1), 357–366. https://doi.org/10.1103/PhysRevA.58.357.
31. Grant, I. P. Relativistic Atomic Structure Calculations. *Comput. Phys. Commun.* **1979**, *17* (1–2), 149–161. https://doi.org/10.1016/0010-4655(79)90077-8.
32. Fischer, C. F.; Godefroid, M.; Brage, T.; Jönsson, P.; Gaigalas, G. Advanced Multiconfiguration Methods for Complex Atoms: I. Energies and Wave Functions. *J. Phys. B At. Mol. Opt. Phys.* **2016**, *49* (18), 182004. https://doi.org/10.1088/0953-4075/49/18/182004.
33. Eissner, W.; Jones, M.; Nussbaumer, H. Techniques for the Calculation of Atomic Structures and Radiative Data Including Relativistic Corrections. *Comput. Phys. Commun.* **1974**, *8* (4), 270–306. https://doi.org/10.1016/0010-4655(74)90019-8.
34. Badnell, N. R. On the Effects of the Two-Body Non-Fine-Structure Operators of the Breit - Pauli Hamiltonian. *J. Phys. B: At. Mol. Opt. Phys.* **1997**, *30* (1), 1. https://doi.org/10.1088/0953-4075/30/1/005.
35. Klapisch, M.; Schwob, J. L.; Fraenkel, B. S.; Oreg, J. The 1s-3p Kb-Like X-Ray Spectrum of Highly Ionized Iron. *J. Opt. Soc. Am.* **1977**, *67* (2), 148–155.
36. Desclaux, J. P. Relativistic Dirac-Fock Expectation Values for Atoms With $Z = 1$ to $Z = 120$. *At. Data Nucl. Data Tables* **1973**, *12* (4), 311–406. https://doi.org/10.1016/0092-640X(73)90020-X.
37. Parpia, F. A.; Froese Fischer, C.; Grant, I. P. GRASP92: A Package for Large-Scale Relativistic Atomic Structure Calculations. *Comput. Phys. Commun.* **1996**, *94* (2–3), 249–271. https://doi.org/10.1016/0010-4655(95)00136-0.
38. Klapisch, M. A Program for Atomic Wavefunction Computations by the Parametric Potential Method. *Comput. Phys. Commun.* **1971**, *2* (5), 239–260. https://doi.org/10.1016/0010-4655(71)90001-4.
39. Bar-Shalom, A.; Klapisch, M.; Oreg, J. HULLAC, an Integrated Computer Package for Atomic Processes in Plasmas. *J. Quant. Spectrosc. Radiat. Transf.* **2001**, *71* (2–6), 169–188. https://doi.org/10.1016/S0022-4073(01)00066-8.
40. Badnell, N. R. A Breit-Pauli Distorted Wave Implementation for Autostructure. *Comput. Phys. Commun.* **2011**, *182* (7), 1528–1535. https://doi.org/10.1016/J.CPC.2011.03.023.
41. Bautista, M. A. Electronic Correlations and Polarizability of the Thomas-Fermi-Dirac-Amaldi Potential: Applications to the Singly Ionized Iron-Peak Species. *J. Phys. B At. Mol. Opt. Phys.* **2008**, *41* (6), 065701. https://doi.org/10.1088/0953-4075/41/6/065701.
42. Gombás, P. Statistische Behandlung des Atoms. In Atoms II/Atome II; Springer: Berlin, Heidelberg, 1956; pp. 109–231. https://doi.org/10.1007/978-3-642-85687-7_2.
43. Froese Fischer, C. General Hartree-Fock Program. *Comput. Phys. Commun.* **1987**, *43* (3), 355–365. https://doi.org/10.1016/0010-4655(87)90053-1.
44. Williams, G. *DPASS21.06*; 2020. https://www.sdu.dk/en/dpass.
45. Montanari, C. C.; Archubi, C. D.; Mitnik, D. M.; Miraglia, J. E. Energy Loss of Protons in Au, Pb, and Bi Using Relativistic Wave Functions. *Phys. Rev. A* **2009**, *79* (3), 032903. https://doi.org/10.1103/PhysRevA.79.032903.
46. Montanari, C. C.; Mitnik, D. M.; Archubi, C. D.; Miraglia, J. E. Energy Loss of Protons in W Using Fully Relativistic Calculations and Mean Excitation Energies of W, Au, Pb, and Bi. *Phys. Rev. A* **2009**, *80* (1), 012901. https://doi.org/10.1103/PhysRevA.80.012901.
47. Montanari, C. C.; Miraglia, J. E.; Arista, N. R. Suppression of Projectile-Electron Excitations in Collisions With a Free-Electron Gas of Metals. *Phys. Rev. A* **2000**, *62* (5), 052902. https://doi.org/10.1103/PhysRevA.62.052902.
48. Ziegler, J. F. *SRIM*; 2013. http://www.srim.org/.

49. Ziegler, J. F.; Ziegler, M. D.; Biersack, J. P. SRIM—The Stopping and Range of Ions in Matter (2010). *Nucl. Instrum. Methods Phys. Res. Sect. B* **2010**, *268* (11), 1818–1823. https://doi.org/10.1016/j.nimb.2010.02.091 (19th International Conference on Ion Beam Analysis).
50. IAEA.; Paul, H.; Montanari, C. C. *Electronic Stopping Power of Matter for Ions Graphs, Data, Comments and Programs*; 1928–2021. https://www-nds.iaea.org/stopping/.
51. Sirotinin, E. I.; Tulinov, A. F.; Khodyrev, V. A.; Mizgulin, V. N. *Nucl. Instrum. Methods Phys. Res. Sect. B* **1984**, *4* (3), 337–345.
52. Grande, P. L.; Schiwietz, G. *CasP version 6.0*; 2021. http://www.casp-program.org/.
53. Matias, F.; Fadanelli, R. C.; Grande, P. L.; Arista, N. R.; Koval, N. E.; Schiwietz, G. Stopping Power of Cluster Ions in a Free-Electron Gas From Partial-Wave Analysis. *Phys. Rev. A* **2018**, *98* (6), 062716. https://doi.org/10.1103/PhysRevA.98.062716.
54. Schinner, A.; Sigmund, P. *DPASS21.06*; 2020. https://www.sdu.dk/en/dpass.
55. Schinner, A.; Sigmund, P. Expanded PASS Stopping Code. *Nucl. Instrum. Methods Phys. Res. Sect. B* **2019**, *460*, 19–26. https://doi.org/10.1016/j.nimb.2018.10.047.
56. Luomajarvi, M. Stopping Powers of Some Metals for 0.3–1.5 MeV Protons. *Radiat. Effects* **1979**, *40* (3), 173–179. https://doi.org/10.1080/00337577908237920.
57. Chumanov, V. Y.; Izmailov, S. Z.; Pokhil, G. P.; Sirotinin, E. I.; Tulinov, A. F. *Phys. Status Solidi A* **1979**, *53* (1), 51–62. https://onlinelibrary.wiley.com/doi/epdf/10.1002/pssa.2210530104.
58. Sirotinin, E. I.; Tulinov, A. F.; Fiderkevich, A.; Shyshkin, K. S. The Determination of Energy Losses From the Spectrum of Particles Scattered by a Thick Target. *Radiat. Effects* **1972**, *15* (3–4), 149–152. https://doi.org/10.1080/00337577208234688.
59. Green, D. W.; Cooper, J. N.; Harris, J. C. Stopping Cross Sections of Metals for Protons of Energies From 400 to 1000 kev. *Phys. Rev.* **1955**, *98* (2), 466–470. https://doi.org/10.1103/PhysRev.98.466.
60. Ogino, K.; Kiyosawa, T.; Kiuchi, T. Stopping Powers for MeV Tritons in Solids. *Nucl. Instrum. Methods Phys. Res. Sect. B* **1988**, *33* (1), 155–157. https://doi.org/10.1016/0168-583X(88)90535-6.
61. Sörensen, H.; Andersen, H. H. Stopping Power of Al, Cu, Ag, Au, Pb, and U for 5–18-MeV Protons and Deuterons. *Phys. Rev. B* **1973**, *8* (5), 1854–1863. https://doi.org/10.1103/PhysRevB.8.1854.
62. Bader, M.; Pixley, R. E.; Mozer, F. S.; Whaling, W. Stopping Cross Section of Solids for Protons, 50–600 kev. *Phys. Rev.* **1956**, *103* (1), 32–38. https://doi.org/10.1103/PhysRev.103.32.
63. Eppacher, C.; Semrad, D. Dependence of Proton and Helium Energy Loss in Solids Upon Plasma Properties. *Nucl. Instrum. Methods Phys. Res. Sect. B* **1992**, *69* (1), 33–38. https://doi.org/10.1016/0168-583X(92)95735-A.
64. Sakamoto, N.; Ogawa, H.; Mannami, M.; Kimura, K.; Susuki, Y.; Hasegawa, M.; Katayama, I.; Noro, T.; Ikegami, H. Stopping Powers of Metallic Elements for High Energy Ions. *Radiat. Effects Defects Solids* **1991**, *117* (1–3), 193–195. https://doi.org/10.1080/10420159108220612.
65. Sakamoto, N.; Shiomi, N.; Ogawa, H.; Ishiwari, R. Stopping Powers of Sn and Pb for 3.0–8.5 MeV Protons. *Nucl. Instrum. Methods Phys. Res. Sect. B* **1986**, *13* (1), 115–118. https://doi.org/10.1016/0168-583X(86)90485-4.
66. Ishiwari, R.; Shiomi, N.; Sakamoto, N. Stopping Powers of Zr, Pd, Cd, in and Pb for 6.5 MeV Protons and Mean Excitation Energies. *Nucl. Instrum. Methods Phys. Res. Sect. B* **1984**, *2* (1), 195–198. https://doi.org/10.1016/0168-583X(84)90187-3.
67. Bischel, H.; Hiraoka, T. Energy Loss of 70 MeV Protons in Elements. *Nucl. Instrum. Methods Phys. Res. Sect. B* **1992**, *66* (3), 345–351. https://doi.org/10.1016/0168-583X(92)95995-4.

68. Eckardt, J. C. Energy Loss and Straggling of Protons and Helium Ions Traversing Some Thin Solid Foils. *Phys. Rev. A* **1978**, *18* (2), 426–433. https://doi.org/10.1103/PhysRevA.18.426.
69. Krist, T.; Mertens, P. Proton Energies at the Maximum of the Electronic Stopping Cross Section in Materials With 57≤Z≤83. *Nucl. Instrum. Methods Phys. Res.* **1983**, *218* (1), 790–794. https://doi.org/10.1016/0167-5087(83)91084-0.
70. Krist, T.; Mertens, P. Stopping Ratios for 30–330 keV Light Ions in Materials With 57≤Z≤83. *Nucl. Instrum. Methods Phys. Res.* **1983**, *218* (1), 821–826. https://doi.org/10.1016/0167-5087(83)91090-6.
71. Arkhipov, E. P.; Gott, Y. V. Slowing Down of 0.5-30 keV Protons in Some Materials. *Soviet J. Exp. Theor. Phys.* **1969**, *29*, 615.
72. Eppacher, C. *Die "effektive Ladung" von schnellen Heliumionen in Metallen* (Ph.D. thesis), Schriften der Johannes-Kepler-Universität Linz, Universitätsverlag Rudolf Trauner, 1995.
73. Valdés, J.; Tamayo, G.; Lantschner, G.; Eckardt, J.; Arista, N. Electronic Energy Loss of Low Velocity H+ Beams in Al, Ag, Sb, Au and Bi. *Nucl. Instrum. Methods Phys. Res. Sect. B* **1993**, *73* (3), 313–318. https://doi.org/10.1016/0168-583X(93)95744-P.
74. Knudsen, H.; Andersen, H. H.; Martini, V. Hydrogen and Helium Stopping Powers of Rare-Earth Metals. *Nucl. Instrum. Methods* **1980**, *168* (1), 41–50. https://doi.org/10.1016/0029-554X(80)91229-X.